Analysis of the Anisotropy of Group Velocity Error Due to the Application of Spatial Finite Difference Schemes to the Solution of the 2D Linear Euler Equations

P. C. Stegeman[1], M. E. Young[2], J. Soria[1] and A. Ooi[3]

[1]Laboratory for Turbulence Research in Aerospace and Combustion, Department of Mechanical and Aerospace Engineering, Monash University, VIC 3800, AUSTRALIA

[2]Air Vehicles Division, Defence Science and Technology Organisation, Fishermans Bend, VIC 3207, AUSTRALIA

[3]Department of Mechanical Engineering, University of Melbourne, Parkville, VIC 3052, AUSTRALIA

Abstract

Numerical differencing schemes are subject to dispersive and dissipative errors, which in one dimension are functions of wavenumber. When these schemes are applied in two or three dimensions, the errors become functions of both wavenumber and the direction of wave propagation. In this paper spectral analysis was used to analyse the magnitude and direction in error of the group velocity of vorticity-entropy and acoustic waves in the solution of the linearised Euler equations in a two-dimensional Cartesian space. The anisotropy in these errors for three schemes were studied as a function of the wavenumber, wave direction, mean flow direction and mean flow Mach number. It was found that the traditional measure of error - the ratio of the magnitudes of the numerical to real group velocities - does not accurately capture the total error for waves which are traveling in an oblique direction to the mean flow. Therefore a second measure of a scheme's error that better represents the total error in the scheme is presented. Numerical experiments were run to provide confirmation of the developed theory.

Introduction

With increased interest in the computation of turbulence and with the advent of computational aeroacoustics (CAA), methods were developed to increase the resolution of finite difference schemes as required for these applications. Formal truncation error provides some indication of the accuracy of a numerical scheme; however, far more information can be obtained from a spectral analysis in which one can identify the resolvable wavenumbers. The use of spectral analysis to assess the resolution of numerical schemes is well established ([7] and [15]). However, the overwhelming majority of analyses on the resolution and accuracy of these schemes have been performed in only one dimension. In some cases schemes were tested for their performance in two dimensions [4, 5, 1, 2, 3], whilst others have anisotropy reduction as a primary motivation [6, 8, 9, 11, 13, 16]. In most cases the analysis of anisotropy in a scheme's error is portrayed by a polar plot of the ratio of numerical phase speed to exact phase speed for a range of wavenumbers. Implicit in such an analysis is the assumption that the waves are aligned with the direction of propagation. This assumption is restrictive and does not apply in general applications. [14] showed how the physical propagation of the waves moves according to group velocity and [12, p.558] asserts that phase velocity is 'totally irrelevant' with regards to the error of wave propagation. Therefore this paper focuses on the use of group velocity to explain the phenomena observed. For the purposes of exploring the anisotropy of finite difference schemes the sixth order central difference scheme (CDS6) is used as an example. The definition of the CDS6 scheme and its equivalent wavenumber as a function of actual wavenumber is commonly found in literature (e.g. [8]) and will not be explicitly defined here. This paper provides an overview of the work found in [10].

Definition of Error Measures

From the linear evolution form of the Euler equations

$$\frac{\partial U'}{\partial t} + A_1 \frac{\partial U'}{\partial x_1} + A_2 \frac{\partial U'}{\partial x_2} = 0, \qquad (1)$$

$$U' = \begin{bmatrix} \rho' \\ u'_1 \\ u'_2 \\ p' \end{bmatrix} \qquad (2)$$

$$A_1 = \begin{bmatrix} \bar{u}_1 & \bar{\rho} & 0 & 0 \\ 0 & \bar{u}_1 & 0 & \frac{1}{\bar{\rho}} \\ 0 & 0 & \bar{u}_1 & 0 \\ 0 & \bar{\rho}\bar{a}^2 & 0 & \bar{u}_1 \end{bmatrix} \qquad (3)$$

$$A_2 = \begin{bmatrix} \bar{u}_2 & 0 & \bar{\rho} & 0 \\ 0 & \bar{u}_2 & 0 & 0 \\ 0 & 0 & \bar{u}_2 & \frac{1}{\bar{\rho}} \\ 0 & 0 & \bar{\rho}\bar{a}^2 & \bar{u}_2 \end{bmatrix}, \qquad (4)$$

where ρ is the fluid density, u_i the velocity components, p the pressure, a the speed of sound, a prime denotes fluctuating quantities and an overbar denotes mean quantities. By applying the continuous and discrete Fourier-Laplace transform to equation (1) we determine the analytical and numerical group velocity (for non diffusive schemes) respectively as

$$u_{g_i} = \bar{u}_i + \frac{\alpha k_i}{\sqrt{k_1^2 + k_2^2}} \qquad (5)$$

and

$$u_{g_i}^\star = \sum_{j=1}^{2} \left(\left\{ u_j + \frac{\alpha \left(k_j^\star \Delta_j \right)}{\sqrt{\left(k_1^\star \Delta_1 \right)^2 + \left(k_2^\star \Delta_2 \right)^2}} \right\} \frac{\partial \left(k_j^\star \Delta_j \right)}{\partial k_i} \right) \qquad (6)$$

where $\bar{u}_i$ is the mean flow velocity vector, k_i is the wavenumber vector, $k_i^\star$ is the equivalent wavenumber vector, Δ_i is the grid spacing vector and α is a selector variable. When $\alpha = 0$ these equations represent the group velocity for the vorticity-entropy waves and when $\alpha = -1$ or $\alpha = 1$ these equations represent the group velocity for the upstream and downstream acoustic waves respectively. The mean speed of sound and density are assumed to be 1 therefore $\bar{u}_i$ is also the Mach vector. The numerical group velocity was derived under the assumption that discretisation is applied only in the spatial domain. As can be seen the numerical group velocity exhibits a strong dependence not only on the equivalent wavenumber but its derivative with respect to the exact wavenumber. We may expect that the group velocity may be zero or propagate in the oblique directions when $\partial(k_1^\star \Delta_1)/\partial k_1 \leq 0$ and/or $\partial(k_2^\star \Delta_2)/\partial k_2 \leq 0$.
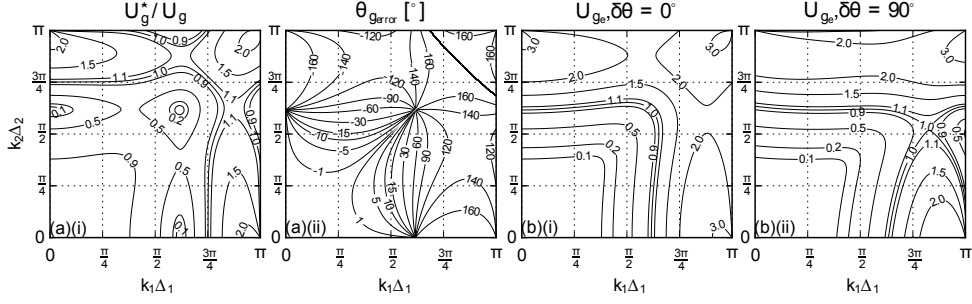
Figure 1: (a)(i) Ratio of modulus; (a)(ii) Absolute phase error; (b)(i-ii) Relative error of the numerical downstream acoustic wave propagation for the CDS6 scheme; (a)(i-ii) and (b)(i) show values for $\delta\theta = 0°$; (b)(ii) show values for $\delta\theta = 90°$. Taken from [10].

The ratio of group velocity magnitudes is often used in literature to determine the dispersion error and is related to the classical measure of relative error in modulus or group velocity magnitudes, which would be equal to $1 - U_g^\star/U_g$. In this case the dispersion error in the given scheme decreases as $U_g^\star/U_g$ approaches 1. However for multidimensional analysis the error in modulus do not account for the difference in the group velocity direction or error in phase. The ratio of group velocity magnitudes and absolute error in phase are defined respectively as

$$\frac{U_g^\star}{U_g} = \frac{||\mathbf{u}_g^\star||}{||\mathbf{u}_g||} \tag{7}$$

and

$$\theta_{g_{error}} = \arctan\left(\frac{\mathbf{u}_g^\star \cdot \mathbf{R}_{-90°}\mathbf{u}_g}{\mathbf{u}_g^\star \cdot \mathbf{u}_g}\right). \tag{8}$$

where $\mathbf{R}_{-90°}$ is the 90° counter-clockwise rotation matrix. Figure 1(a)(i-ii) represent these respective errors for the downstream acoustic waves ($\alpha = 1$) for any given relative wavenumber vector. As with the classical anisotropy error plots the wave content is aligned with the mean velocity direction which has a magnitude of $\bar{U} = 0.5$.

As expected due to the large errors in phase at higher wavenumbers the total error in the schemes is not accurately described by the ratio of group velocity magnitudes. To determine an appropriate error measure we must consider the error in modulus and phase to include the multidimensional effects. It is therefore more appropriate, in comparing numerical schemes, to use the relative magnitude of the error vector, $\mathbf{u}_{g_e} = \mathbf{u}_g^\star - \mathbf{u}_g$,

$$U_{g_e} = \frac{||\mathbf{u}_{g_e}||}{||\mathbf{u}_g||} = \frac{||\mathbf{u}_g^\star - \mathbf{u}_g||}{||\mathbf{u}_g||}. \tag{9}$$

This metric better captures the difference between the real and numerical group velocity vectors as it includes both the error in modulus and error in phase. It more accurately describes the effectiveness of a scheme for the multidimensional Euler equations in a single variable. Unlike the prior approach the dispersion error in the given scheme decreases as U_{g_e} approaches 0. Figures 1(b)(i-ii) represent this error for the upstream acoustic waves when the velocity direction is aligned ($\delta\theta = 0°$) and perpendicular ($\delta\theta = 0°$) to the wavenumber content direction.

Comparison of Error Measures

From this analysis we found that the classical error analysis under predicts the total error present when the wavenumber content is not aligned with the mean velocity direction. However the maximum error occurs when the wavenumber content and velocity direction are aligned along the principle axes and therefore reduces to the classical 1D analysis. For the acoustic wave

propagation this may be seen in figure 2 which plots the maximum value of $1 - U_g^\star/U_g$ and U_{g_e} of a wave traveling in any direction for the CDS6 scheme and the multi-dimensionally optimized scheme (MDS6) found in [8].
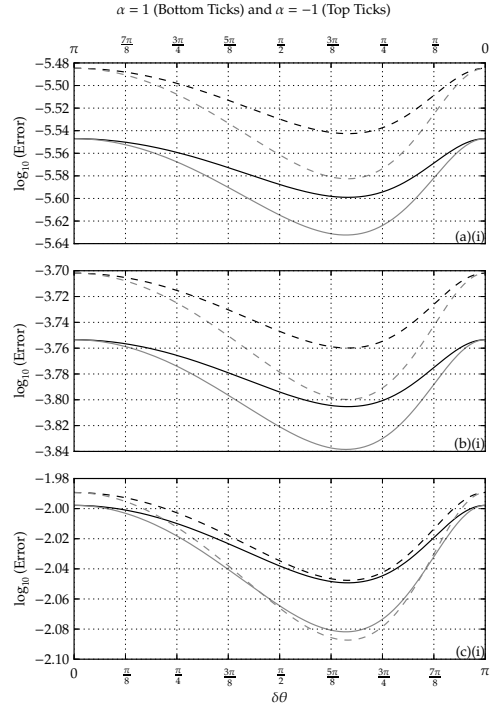

Figure 2: Comparison of the maximum error for a wave with any direction (θ_w) with respect to the difference between the mean flow velocity direction and wave direction ($\delta\theta$). (a) to (c) show results for waves with wavenumbers of $\pi/16$, $\pi/8$, and $\pi/4$, respectively. Solid lines represent the CDS6 scheme and dashed lines represent the MDS6 scheme. Dark lines represent the multidimensional error and the grey lines represent the standard error. $\bar{U} = 1.0$. Taken from [10].

As expected these cases show that the multidimensional error is greater than the standard error due to the inclusion of the error in phase. However when the wave direction is aligned with the direction of mean flow the maximum of both errors are equivalent. This is due to the maximum error in these cases occurring along the $k_1\Delta_1$ and $k_2\Delta_2$ axes where the solution reduces to a 1D problem and the error in phase is zero. Both errors decrease as the mean flow velocity diverges from the wavenumber content direction and at faster rates for higher mean flow velocities.

A more in depth analysis of the relationship between the u_j and $k_j\Delta_j$ vector and $\partial_{k_i}\left(k_j^\star\Delta_j\right)$ matrix is required to understand the cause of such results.

Numerical Experiment

This section compares the propagation of an initial Gaussian profile using the CDS6 numerical methods analysed under the two-dimensional linearised Euler equations in Cartesian coordinates. They are compared to the predictions made using group velocity as described in equation (6). For all numerical results the fourth-order Runge-Kutta time discretisation scheme was used with a maximum CourantFriedrichsLewy number of approximately 0.01. The grid spacing was set at $\Delta_1 = \Delta_2 = 0.036$ with a time step interval of $\Delta_t = 0.001$. The spatial domain was $-18 \leq x_1 \leq 18$ and $-18 \leq x_2 \leq 18$, which provided sufficient clearance between the solution and boundaries. All results are given for a time of $t = 4$ s. The mean density, pressure and velocity for all simulations were $\bar{\rho} = 1$, $\bar{p} = 1$ and $\bar{U} = 0.5$ in a direction $30°$ counter-clockwise from the x-axis.

A Gaussian profile profile theoretically contains all frequencies such that the component waves are expected to propagate in all directions about the mean flow velocity. The initial perturbation was defined as

$$U' = \begin{bmatrix} 0.0 \\ 0.0 \\ 0.0 \\ 0.1 \end{bmatrix} e^{-g\left(x_1^2 + x_2^2\right)}. \tag{10}$$

A value of $g = 275$ was chosen to reduce aliasing by setting the relative amplitude of the component waves with the highest wavenumber (Nyquist limit) is approximately 10% of the base amplitude. These results show the spread of dispersion errors for the entire wavenumber range of the mesh for each of the given schemes.

Figure 3 shows the results for the CDS6 scheme. Sub-figure (a) is a plot of the unfiltered density field and the range of analytical positions, represented by the dotted lines, of the vorticity-entropy waves with the wavenumber content aligned along the range of $-180° < \delta\theta < 180°$ at selected wavenumber magnitudes. The extent of the waves show the spread of possible propagation as predicted by the spectral analysis. Sub-figures (c) to (d) are plots of the Gaussian bandpass filtered density field defined as

$$\hat{U}'_{\text{Filtered}}(k_1, k_2) = \hat{U}'(k_1, k_2)\, e^{\frac{-(\Delta k - (\Delta k)_c)^2}{2\sigma^2}} \tag{11}$$

where $\Delta k = \sqrt{(\Delta_1 k_1)^2 + (\Delta_2 k_2)^2}$ is the magnitude of the relative wavenumber components, $\sigma = \pi/20$ and $(\Delta k)_c$ is the center wavenumber of the filter. The dotted lines represent the analytical position of the accoustic waves with a wavenumber content of $(\Delta k)_c$ along the range of $-180° < \delta\theta < 180°$. As may be seen the analytical theory developed compares very well with the numerical results even though the spread of waves exhibits complicated patterns at larger wavenumbers. Waves with larger deviation from the real propagation position correspond to those with higher wavenumbers.

Conclusions

A spectral analysis of the 2D linearized Euler equations has been completed in order to predict the error in magnitude and direction of the group velocity of vorticity-entropy and acoustic waves. A different measure of the group velocity error — the relative magnitude of the error vector between the numerical and real group velocities — was used to account for the directional error of wave propagation. The comparison shows that the traditional measure of error — the ratio of the magnitudes of the numerical to real group velocities — is lower for flow velocity directions oblique to that of the wave propagation direction. Such behavior in numerical wave propagation cannot be reflected in the typical anisotropy diagrams seen in current literature and is important with regards to the understanding of dispersion error in multidimensional finite difference solutions of the Euler and Navier-Stokes equations.

References

[1] Chiu, P. H. and Sheu, T. W. H., On the development of a dispersion-relation-preserving dual-compact upwind scheme for convection-diffusion equation, *J. Comput. Phys.*, **228**, 2009, 3640–3655.

[2] Chu, P. C. and Fan, C., A three-point combined compact difference scheme, *J. Comput. Phys.*, **140**, 1998, 370–399.

[3] De, A. K. and Eswaran, V., Analysis of a new high resolution upwind compact scheme, *J. Comput. Phys.*, **218**, 2006, 398–416.

[4] Lele, S., Compact finite difference schemes with spectral-like resolution, *J. Comput. Phys.*, **103**, 1992, 16–42.

[5] Li, Y., Wavenumber-extended high order upwind biased finite difference schemes for convective scalar transport, *J. Comput. Phys.*, **133**, 1997, 235–255.

[6] Lin, R. K. and Sheu, W. H., Application of dispersion-relation-preserving theory to develop a two-dimensional convection-diffusion scheme, *J. Comput. Phys.*, **208**, 2005, 493–526.

[7] Moin, P., *Fundamentals of Engineering Numerical Analysis*, Cambridge University Press, Cambridge, 2001.

[8] Sescu, A., Hixon, R. and Afjeh, A., Multidimensional optimization of finite difference schemes for computational aeroacoustics, *J. Comput. Phys.*, **227**, 2008, 4563–4588.

[9] Shen, G. and Cangellaris, A. C., A new FDTD stencil for reduced numerical anisotropy in the computer modeling of wave phenomena, *Int. J. R.F. Microw. Comput. Aided Engin.*, **17**, 2007, 447–454.

[10] Stegeman, P. C., Young, M. E., Soria, J. and Ooi, A., Analysis of the anisotropy of group velocity error due to spatial finite difference schemes from the solution of the 2d linear euler equations, *International Journal for Numerical Methods in Fluids*, **Early View**.

[11] Sun, G. and Trueman, C. W., Suppression of numerical anisotropy and dispersion with optimized finite-difference time-difference methods, *IEEE Transactions on Antennas and Propagation*, **53**, 2005, 4121–4128.

[12] Tam, C. K. W., Computational aeroacoustics: an overview of computational challenges and applications, *Int. J. Comput Fluid Dyn.*, **18**, 2004, 547–567.
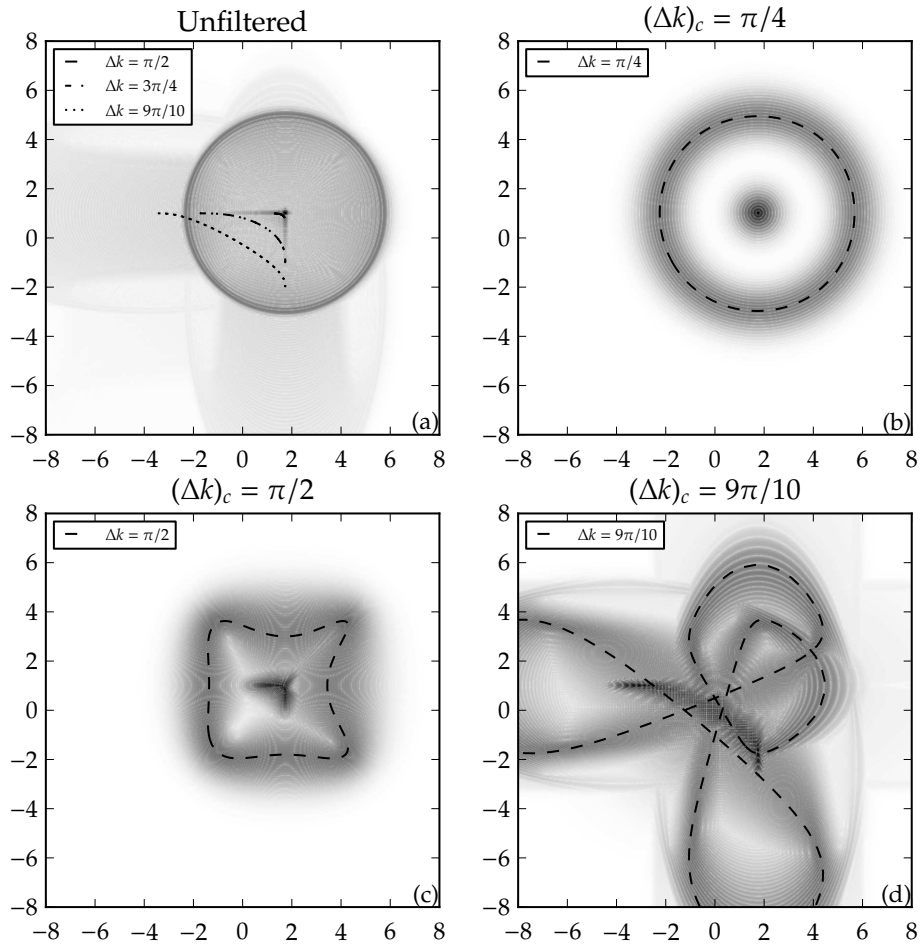
Figure 3: Plot of the numerical results of the initial Gaussian profile solution to the linearised Euler equations using the CDS6 scheme. Taken from [10].

[13] Tam, C. K. W. and Webb, J. C., Radiation boundary condition and anisotropy correction for finite difference solutions of the Helmholtz equation, *J. Comput. Phys.*, **113**, 1994, 122–133.

[14] Trefethen, L., Group velocity in finite difference schemes, *SIAM Review*, **24**, 1982, 113–136.

[15] Vichnevetsky, R. and Bowles, J., *Fourier Analysis of Numerical Approximations of Hyperbolic Equations*, SIAM, Philadelphia, 1982.

[16] Zingg, D. W. and Lomax, H., Finite-difference schemes on regular triangular grids, *J. Comput. Phys.*, **108**, 1993, 306–313.